11-2017

Synthesis and reductive chemistry of bimetallic and trimetallic rare-earth metallocene hydrides with (C5H4SiMe3)1− ligands

Megan T. Dumas
University of California, Irvine

Guo P. Chen
University of California, Irvine

Jasper Y. Hu
University of California, Irvine

Mitchell A. Nascimento
University of Windsor

Jeremy M. Rawson
University of Windsor

See next page for additional authors

For the special issue of the Journal of Organometallic Chemistry, "Organometallic Chemistry of Polynuclear Metal Complexes," dedicated to Editor Rick Adams

Synthesis and Reductive Chemistry of Bimetallic and Trimetallic Rare-Earth Metallocene Hydrides with $(C_5H_4SiMe_3)^{1-}$ Ligands

Megan T. Dumas,[†] Guo P. Chen,[†] Jasper Y. Hu,[†] Mitchell A. Nascimento,[‡] Jeremy M. Rawson,[‡]* Joseph W. Ziller,[†] Filipp Furche,[†]* and William J. Evans[†]*

[†]Department of Chemistry, University of California, Irvine, California 92697-2025, United States and [‡]Department of Chemistry & Biochemistry, University of Windsor, Windsor, Ontario, N9B 3P4 CANADA

Email: wevans@uci.edu, filipp.furche@uci.edu, jmrawson@uwindsor.ca

*To whom correspondence should be addressed.

Dedicated to Professor Rick Adams for his extensive and continuous contributions to inorganic and organometallic chemistry and the advancement of polymetallic cluster chemistry.

ABSTRACT: The reductive chemistry of $[Cp'_2Ln(\mu\text{–}H)(THF)_x]_y$ [Ln = Y, Dy, Tb; Cp' = $(C_5H_4SiMe_3)^{1-}$; x = 2, 0 and y = 2, 3] was examined to determine if these hydrides would be viable precursors for $4f^n5d^1$ Ln^{2+} ions that could form $5d^1$-$5d^1$ metal–metal bonded complexes. The hydrides were prepared by reaction of the chlorides, $[Cp'_2Ln(\mu\text{–}Cl)]_2$, **1-Ln**, with allylmagnesium chloride to form the allyl complexes, $[Cp'_2Y(\eta^3\text{–}C_3H_5)(THF)]$, **2-Ln**, which were hydrogenolyzed. The solvent-free reaction of solid **2-Ln** with 60 psi of H_2 gas in a Fischer-Porter apparatus produced, in the Y case, the trimetallic species, $[Cp'_2Y(\mu\text{–}H)]_3$, **3-Y**, and in the

Dy and Tb cases, the bimetallic complexes $[Cp'_2Ln(\mu\text{–}H)(THF)]_2$, **4-Ln** (Ln = Dy, Tb). The latter complexes could be converted to **3-Dy** and **3-Tb** by heating under vacuum. Isopiestic data indicate that **3-Y** solvates to **4-Y** in THF. Reductions of **4-Y**, **4-Dy**, and **4-Tb** with KC_8 in the presence of a chelate such as 2.2.2-cryptand or 18-crown-6 all gave reaction products with intense dark colors characteristic of Ln^{2+} ions. In the yttrium case, with either chelating agent, the dark green product gives a rhombic EPR spectrum (g_1 = 2.01, g_2 = 1.99, g_3 = 1.98, A = 24.1 G) at 298 K. However, the only crystallographically-characterizable products obtainable from these solutions were Ln^{3+} polyhydride anion complexes of composition, $[K(chelate)]\{[Cp'_2Ln(\mu\text{–}H)]_3(\mu\text{–}H)\}$. Reduction of **1-Y** with KC_8 in the presence of 2.2.2-cryptand also yields an intensely colored product with an axial EPR spectrum ($g_x = g_y$ = 2.05, $A_x = A_y$ = 35.5 G; g_z = 2.07, A_z = 34.5) similar to that of $(Cp'_3Y)^{1-}$ ion, but crystals were not obtained from this system.

1. INTRODUCTION

Recent results in reductive rare-earth metal chemistry have shown that the +2 oxidation state has been isolated for yttrium and all the lanthanides (except radioactive Pm) in the tris(cyclopentadienyl) ligand environments shown in eq 1.[1,2,3,4] Density functional theory (DFT) calculations indicate that in this trigonal environment, a d_z^2 orbital is low enough in energy for the new +2 ions to adopt a $4f^n5d^1$ ground state with the lanthanides and a $4d^1$ electron configuration for yttrium.[4,5,6]

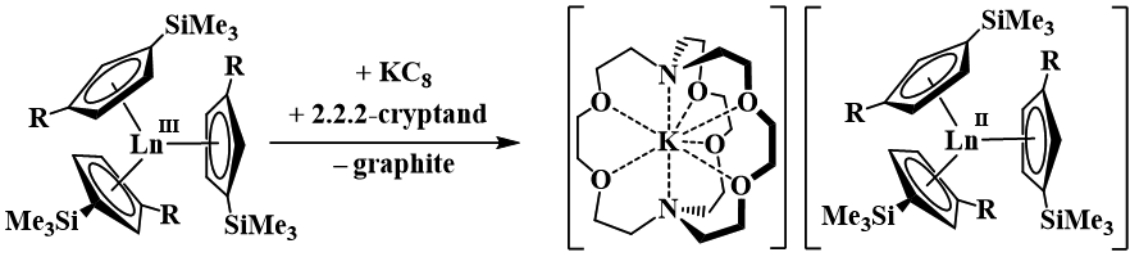

(1)

R = H, Ln = Y, La, Ce, Pr, Nd, Gd, Tb, Dy, Ho, Er, and Lu
R = $SiMe_3$ Ln = La and Ce

The $5d^1$ character of this electron configuration raises the possibility of generating rare-earth metal complexes containing Ln−Ln bonds. Traditionally, Ln−Ln bonding is considered unlikely due to the limited radial extension of the 4f orbitals. In the $(Cp'_3Ln)^{1-}$ and $(Cp''_3Ln)^{1-}$ complexes (Cp' = $C_5H_4SiMe_3$; Cp'' = $C_5H_3(SiMe_3)_2$), however, the additional electron is in a d_z^2 orbital perpendicular to the trigonal plane of the three ring centroids. Given the steric protection of the three cyclopentadienyl rings, $(Cp'_3Ln)^{1-}$ and $(Cp''_3Ln)^{1-}$ are not ideal complexes for forming bimetallic metal–metal bonded species. In contrast, it was not known if bimetallic complexes like $[(C_5R_5)_2Ln(\mu\text{–}X)]_2$ would have the appropriate geometries to lower a d orbital such that $4f^n5d^1$ electron configurations would be the ground state. As described here, density functional theory (DFT) calculations on $[Cp'_2Y(\mu\text{–}Cl)]_2$ and $[Cp'_2Y(\mu\text{–}H)]_2$ suggested that reduction of these species could possibly lead to Y–Y bonds. The hydrides are particularly interesting candidates since hydride ligands in rare-earth complexes are already involved in electron deficient three-center two-electron bonds,[7,8] which could have a low-lying non-bonding orbital.

Yttrium was chosen initially since its I = ½ nuclear spin is useful in NMR and EPR spectroscopic studies and $(Cp')^{1-}$ was chosen since it has allowed the stabilization of d_z^2 orbital and isolation of the +2 oxidation state to all the lanthanides and yttrium.[2,3,4,6] Although bimetallic rare-earth metallocene hydrides such as $[(C_5H_5)_2Y(\mu\text{–}H)(THF)]_2$ have been known

since 1982,[9] the $(Cp')^{1-}$-ligated analogs had not previously been reported in the literature. As a result, multi-step syntheses of new rare-earth metal hydride complexes had to be developed to provide the starting materials including syntheses of the paramagnetic Dy^{3+} (μ = 10.6 μ_B) and Tb^{3+} (μ = 9.7 μ_B) complexes that required crystallographic verification at each step. Reported here are the DFT calculations that originated this project as well as the synthesis of the hydrides, their reductive chemistry, and the polymetallic polyhydride complexes that were isolated from the reduction reactions.

2. RESULTS AND DISCUSSION

DFT Calculations. DFT calculations show that the LUMO of the trivalent $[Cp'_2Y^{III}(\mu\text{–}H)]_2$ and the HOMOs of the mixed valent $[Cp'_2Y^{III}(\mu\text{–}H)_2Y^{II}Cp'_2]^{1-}$ and the divalent $\{[Cp'_2Y^{II}(\mu\text{–}H)]_2\}^{2-}$, Figure 1, are overlapping yttrium d orbitals, which suggests that the reduction of $[Cp'_2Y(\mu\text{–}H)]_2$ could lead to complexes with metal–metal bond character between the two yttrium ions. The calculated Y–Y distances corroborate the metal–metal bonding: the distance decreases from 3.52 Å in the neutral species $[Cp'_2Y(\mu\text{–}H)]_2$ to 3.46 Å and 3.48 Å in the negatively charged $\{[Cp'_2Y(\mu\text{–}H)]_2\}^{1-}$ and $\{[Cp'_2Y(\mu\text{–}H)]_2\}^{2-}$, respectively. Similar Y–Y bonds are predicted for the bimetallic chloride complexes, Figure 2, where the Y–Y distance decreases from 4.03 Å in $[Cp'_2Y(\mu\text{–}Cl)]_2$ to 3.79 Å and 3.59 Å in $\{[Cp'_2Y(\mu\text{–}Cl)]_2\}^{1-}$ and $\{[Cp'_2Y(\mu\text{–}Cl)]_2\}^{2-}$, respectively. Applying Boys orbital localization[10] to $\{[Cp'_2Y(\mu\text{–}H)]_2\}^{2-}$, we obtained localized molecular orbitals that resemble the three-center two-electron bonds in B_2H_6, Figure 3. In addition, the localization procedure mixes some H contribution into the Y–Y bonding orbital, Figure 4, making its bonding character more prominent.

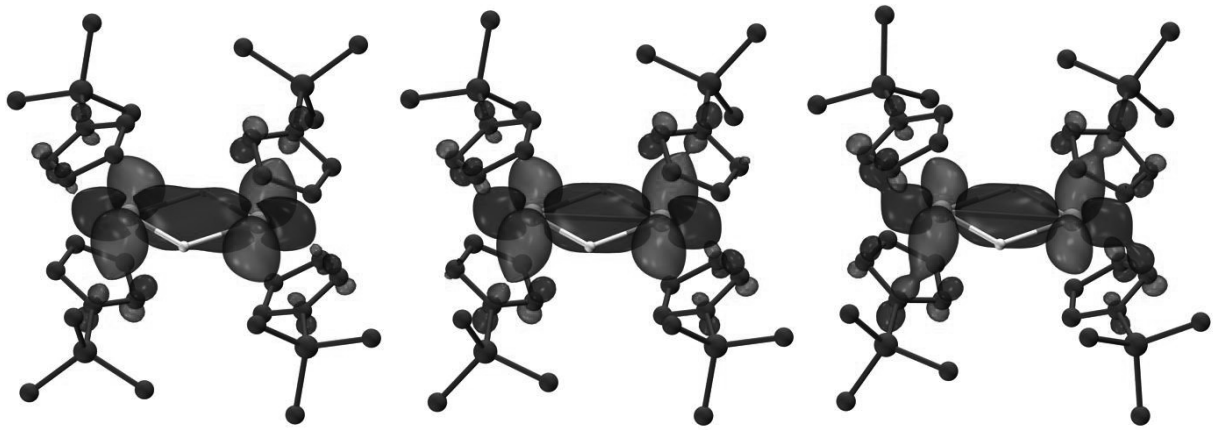

Figure 1. LUMO of $[Cp'_2Y(\mu\text{–}H)]_2$ (left), HOMO of $\{[Cp'_2Y(\mu\text{–}H)]_2\}^{1-}$ (middle), and HOMO of $\{[Cp'_2Y(\mu\text{–}H)]_2\}^{2-}$ (right) with a contour value of 0.04. Hydrogen atoms in Cp' rings are omitted for clarity.

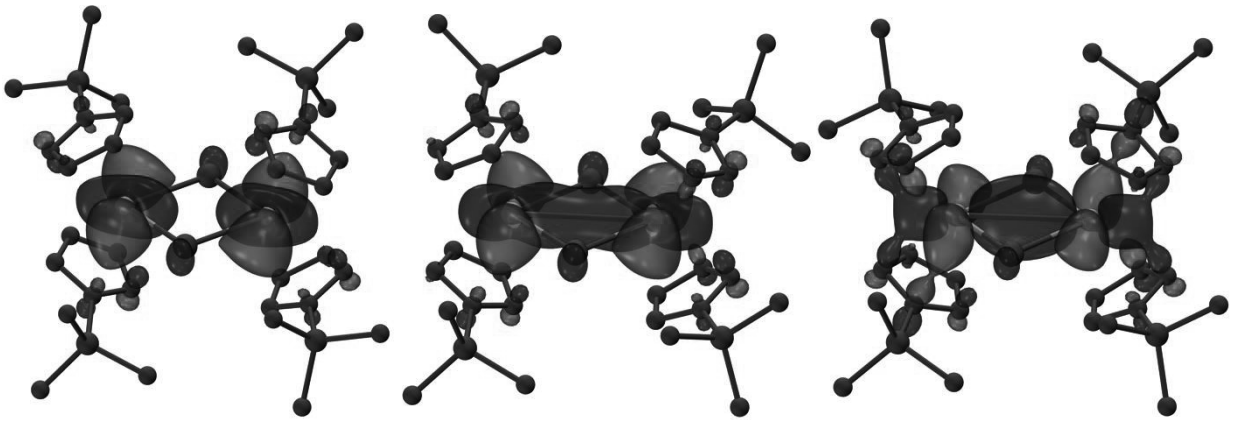

Figure 2. LUMO of $[Cp'_2Y(\mu\text{–}Cl)]_2$ (left), HOMO of $\{[Cp'_2Y(\mu\text{–}Cl)]_2\}^{1-}$ (middle), and HOMO of $\{[Cp'_2Y(\mu\text{–}Cl)]_2\}^{2-}$ (right) with a contour value of 0.04. Hydrogen atoms are omitted for clarity.

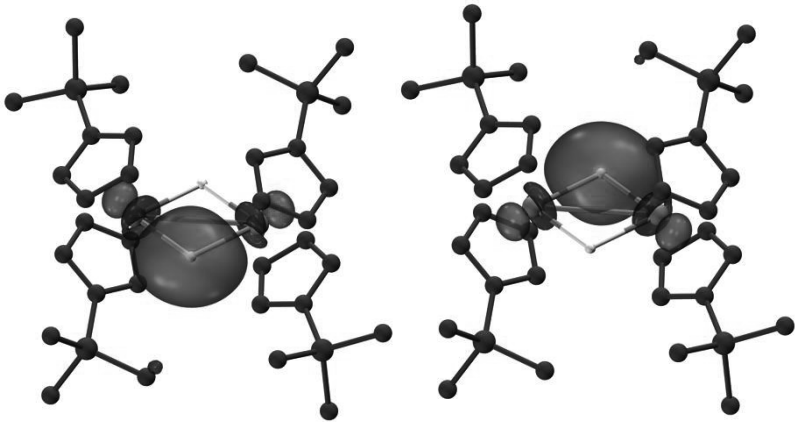

Figure 3. Three-center two-electron localized molecular orbitals of $\{[Cp'_2Y(\mu\text{–}H)]_2\}^{2-}$ with a contour value of 0.04. Hydrogen atoms in Cp' rings are omitted for clarity.

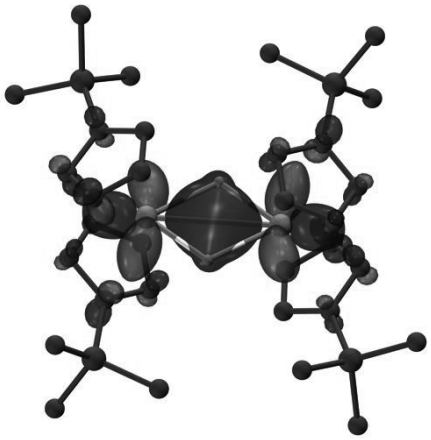

Figure 4. Y–Y bonding localized molecular orbital of $\{[Cp'_2Y(\mu\text{–}H)]_2\}^{2-}$ with a contour value of 0.04. Hydrogen atoms in Cp' rings are omitted for clarity.

Synthesis of Bridging Hydride Complexes. The synthesis of the hydride complexes was accomplished by hydrogenolysis of allyl precursors obtained from the bridging chlorides as shown in Scheme 1. The bridging chlorides, $[Cp'_2Ln(\mu\text{–}Cl)]_2$, **1-Ln** (Ln = Y, Tb, Dy), were

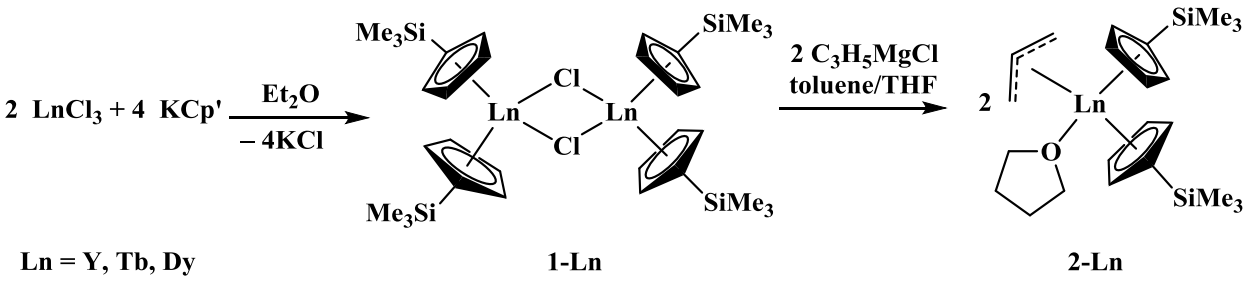

Scheme 1. Synthesis of $[Cp'_2Ln(\mu\text{–}Cl)]_2$, **1-Ln**, and $Cp'_2Ln(\eta^3\text{–}C_3H_5)(THF)$, **2-Ln** (Cp' = $C_5H_4SiMe_3$).

synthesized by treating anhydrous $LnCl_3$ with 2 equivalents of KCp'. The paramagnetic dysprosium and terbium complexes were characterized by X-ray crystallography, Figure 5, and found to have conventional bimetallic structures. These structures are isomorphous with the yttrium,[11] lutetium,[12] ytterbium,[13] and samarium[14] analogues. Their structural parameters are summarized in Table S3 in the Supplementary Content.

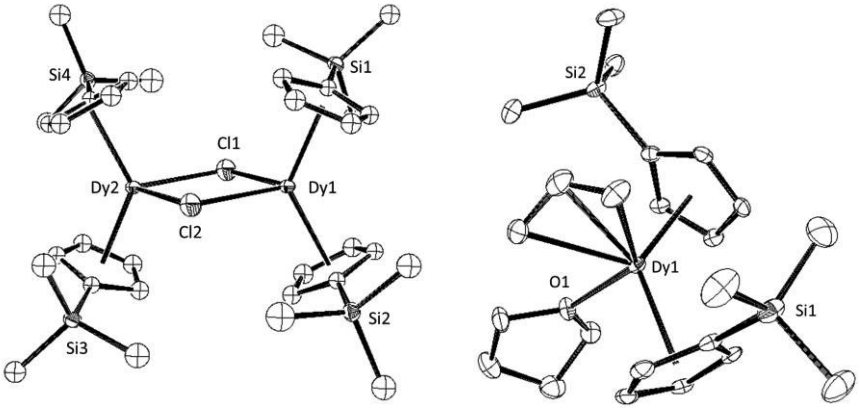

Figure 5. ORTEP depiction of $[Cp'_2Dy(\mu\text{–}Cl)]_2$, **1-Dy** (left), and $Cp'_2Dy(\eta^3\text{–}C_3H_5)(THF)$, **2-Dy** (right), with thermal ellipsoids drawn at the 50% probability level. Hydrogen atoms and co-crystallized solvent molecules have been omitted for clarity. Complexes **1-Tb**, **2-Y**, and **2-Tb** are isomorphous.

Treatment of $[Cp'_2Ln(\mu\text{–}Cl)]_2$ with 2 equivalents of allylmagnesium chloride $(C_3H_5)MgCl$ yielded $Cp'_2Ln(\eta^3\text{–}C_3H_5)(THF)$, **2-Ln** (Ln = Y, Tb, Dy), Scheme 1. These complexes

crystallized as monometallic THF adducts as determined by X-ray crystallography, Figure 5. Bond distances and angles were unexceptional (Table S7). In contrast, the reaction of $[Cp'_2Lu(\mu\text{–}Cl)]_2$ with 2 equivalents of $(C_3H_5)MgCl$ gave the unsolvated tetramer, $[Cp'_2Lu(\eta^3\text{–}C_3H_5)]_4$.[11]

Complexes **2-Ln** (Ln = Dy, Tb, Y) were treated with 60 psi of H_2 gas using a Fischer-Porter pressure reactor in the absence of solvent, Scheme 2. The reaction of solid **2-Y** with 60 psi of H_2 gas produced a white solid identified by X-ray crystallography as the trimetallic complex $[Cp'_2Y(\mu\text{–}H)]_3$, **3-Y**, Figure 6. This is analogous to the previously reported $[(1,3\text{-}Me_2C_5H_3)_2Y(\mu\text{–}H)]_3$.[15]

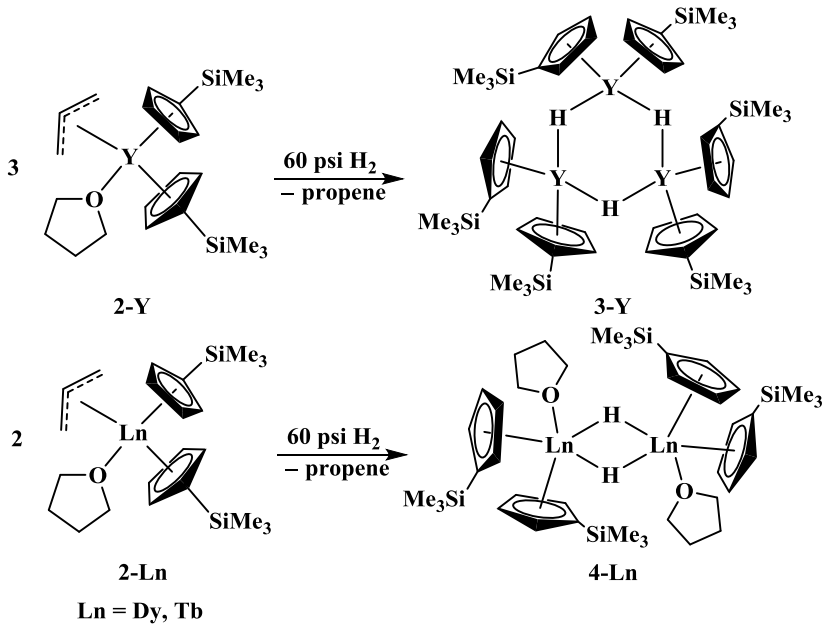

Scheme 2. Reactions between **2-Y** and **2-Ln** (Ln = Dy, Tb) with 60 psi of H_2.

In contrast, treatment of solid **2-Ln** (Ln = Dy, Tb) with 60 psi of H_2 gas produced colorless crystals identified by X-ray crystallography as the solvated bimetallic complexes $[Cp'_2Ln(\mu\text{–}H)(THF)]_2$, **4-Ln**, Scheme 2, (Ln = Dy, Tb), Figure 7. These are analogous to [(1,3-

$Me_2C_5H_3)_2Y(\mu$–H)(THF)]$_2$.[15] Structural details of **4-Ln** are given in the Supplementary Content (S16).

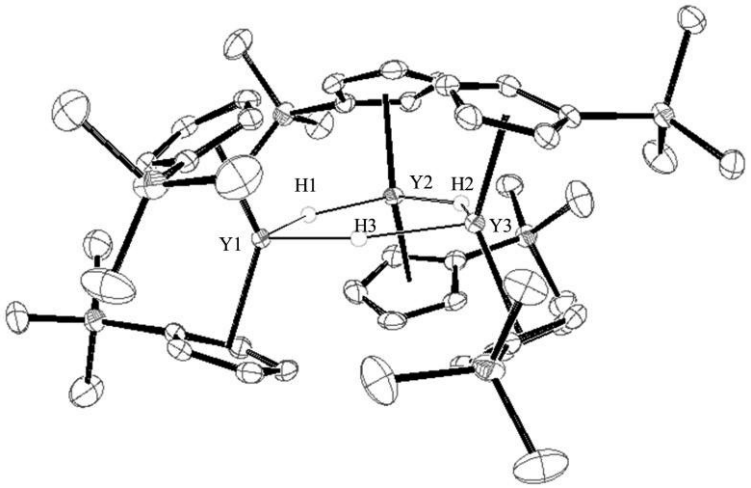

Figure 6. ORTEP depiction of [Cp'$_2$Y(μ–H)]$_3$, **3-Y**, with thermal ellipsoids drawn at the 50% probability level. Co-crystallized solvent and hydrogen atoms, except for the bridging hydride ligands, have been omitted for clarity. Complexes **3-Dy**, and **3-Tb** are isomorphous.

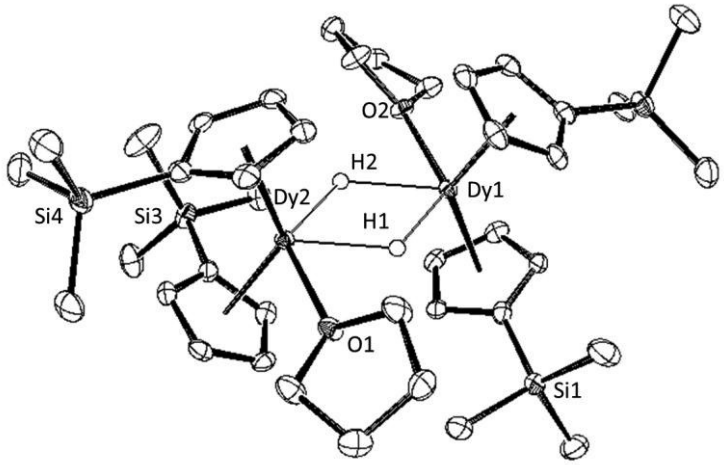

Figure 7. ORTEP depiction of [Cp'$_2$Dy(μ–H)(THF)]$_2$, **4-Dy**, with thermal ellipsoids drawn at the 50% probability level. Hydrogen atoms, except for the bridging hydride ligands, have been omitted for clarity. Complex **4-Tb** is isomorphous.

Initial attempts to expose solutions of **2-Y** to 1 atmosphere of H_2 gas produced crystals of [Cp'$_2$Y(THF)]$_2$(μ–O), **5-Y,** Figure 8, upon workup. While the source of oxygen is unknown, **5-**

Y was consistently observed in solution phase hydrogenolysis reactions via ^{1}H NMR spectroscopy with yields estimated at 20-50% based on the trimethylsilyl peaks. In contrast, this impurity was not formed in the solvent-free gas/solid synthesis of **3-Y**. However, another unanticipated polymetallic product, $[Cp'_2Tb(\mu\text{–}H)]_2(\mu\text{–}H)[Mg(THF)_2](\mu\text{–}H)$, **6-Tb**, Figure 8, was obtained from the reaction between solid **2-Tb** and dihydrogen gas. The sample containing **2-Tb** evidently had residual magnesium present from step 2 in Scheme 1.

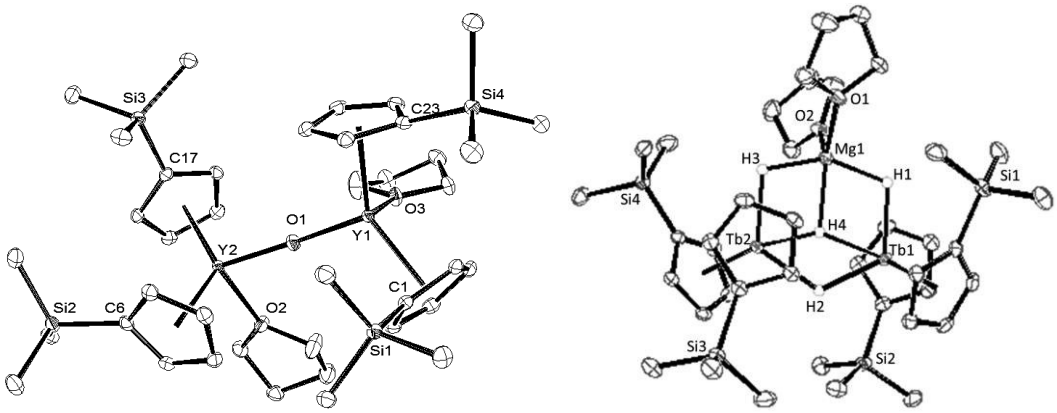

Figure 8. ORTEP depiction of $[Cp'_2Y(THF)]_2(\mu\text{–}O)$, **5-Y**, and $[Cp'_2Tb(\mu\text{–}H)]_2(\mu\text{–}H)[Mg(THF)_2](\mu\text{–}H)$, **6-Tb**, with thermal ellipsoids drawn at the 50% probability level. Hydrogen atoms, except for the bridging hydride ligands, have been omitted for clarity.

Signer isopiestic molecular weight studies of **3-Y** in THF gave a molecular weight of *ca.* 920 g/mol compared to 1093 g/mol for **3-Y** and 873 g/mol for **4-Y**.[16] This suggests that the trimer converts to the bimetallic **4-Y** in THF. The reverse transformation was demonstrated for **4-Dy** and **4-Tb**: desolvation occurs at 10^{-5} torr at 70 °C over 4-5 days. The mass loss of about

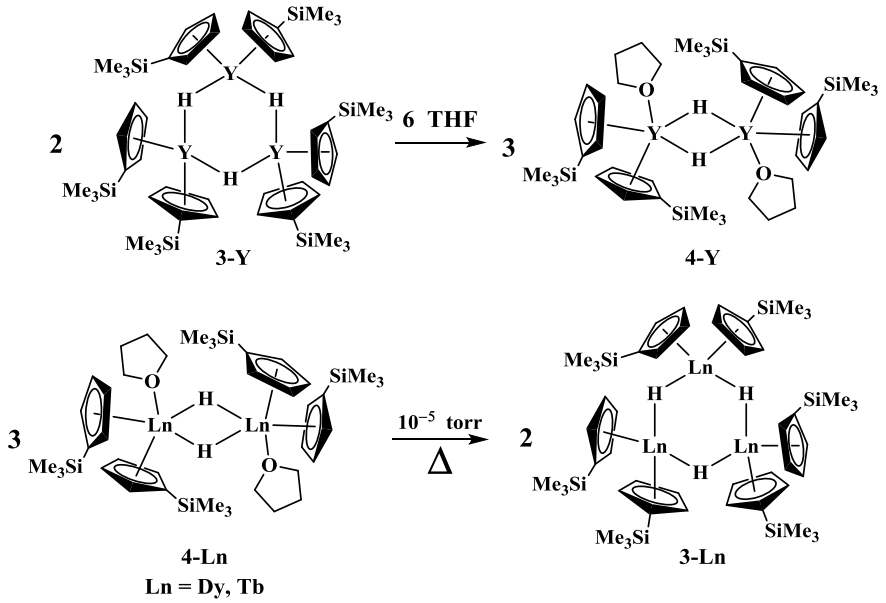

Scheme 3. Conversion between **4-Ln** and **3-Ln**.

14% was consistent with the percent mass of THF present in **4-Ln**. Recrystallization of the desolvated complexes from hexane and toluene produced crystals of **3-Dy** and **3-Tb** identified by X-ray crystallography, Scheme 3, Figure 6. Structural details are given in the Supplementary Content (S13).

Reduction of Bridging Hydride Complexes. The reduction of **4-Y** with one equivalent of KC_8 in the presence of one equivalent of 2.2.2-cryptand (crypt) or 18-crown-6 (crown) in THF produced an intensely colored solution typical of Y^{2+} complexes.[3,4,5] The UV-vis spectrum of the dark green solution had a

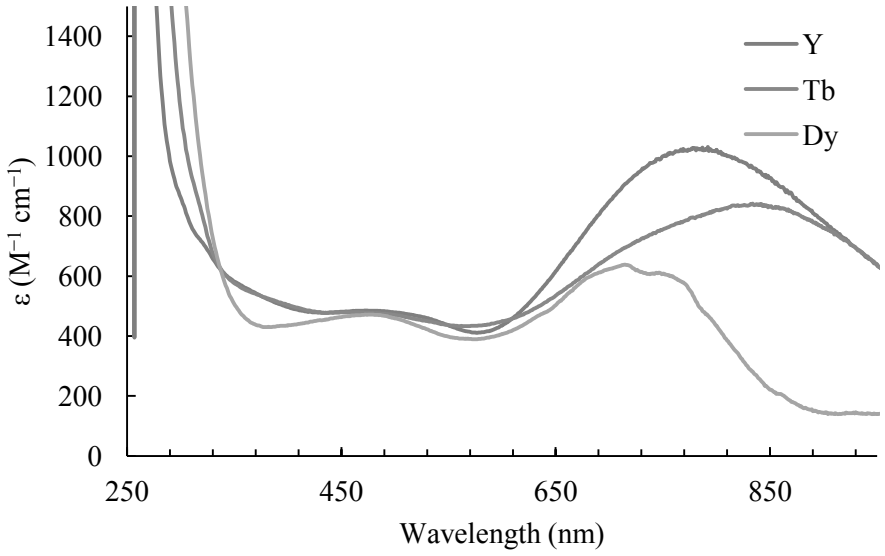

Figure 9. UV-vis spectra of **4-Ln** reduction products: **7-Y** (λ = 794 nm; ε = 1000 $M^{-1}cm^{-1}$), **7-Tb** (λ = 837 nm; ε = 840 $M^{-1}cm^{-1}$), and **7-Dy** (λ = 715 nm; ε = 640 $M^{-1}cm^{-1}$).

broad absorbance at 794 nm with an extinction coefficient of approximately 1000 M^{-1} cm^{-1} based on the moles of yttrium present in the sample, Figure 9. In comparison, [K(crown)][Cp'$_3$Y] and [K(crypt)][Cp'$_3$Y] have absorptions at 530 nm (ε = 2500 $M^{-1}cm^{-1}$) and 520 nm (ε = 4500 $M^{-1}cm^{-1}$).[3,4,5,6]

The EPR spectra of the dark green product, **7-Y**, at 77 K and 298 K are shown in Figure 10. Solution simulations were performed using Winsim[17] whereas frozen spectra were simulated using PIP4WIN.[18] This product displays a broad spectrum around g = 1.983 in good agreement with the weighted average of the principal anisotropic g-tensor components (1.987), Table 1. A low intensity low field feature attributed to a minor impurity was also observed in both fluid and frozen solution spectra, but does not significantly hamper interpretation of the major spectroscopic features. The assorted shoulders and inflection points in the first derivative spectrum are better resolved in the second derivative spectrum shown in Figure 11 with it simulation. This permitted determination of the coupling pattern as a doublet (8.7 G) of 1:2:1

triplets (6.4 G) of 1:2:1 triplets (2.9 G) through simulation, Table 1. The precise origin of this coupling is uncertain in light of the unknown structure of this product (see below). The frozen solution spectrum exhibited axial symmetry with a small hyperfine coupling to the parallel component.

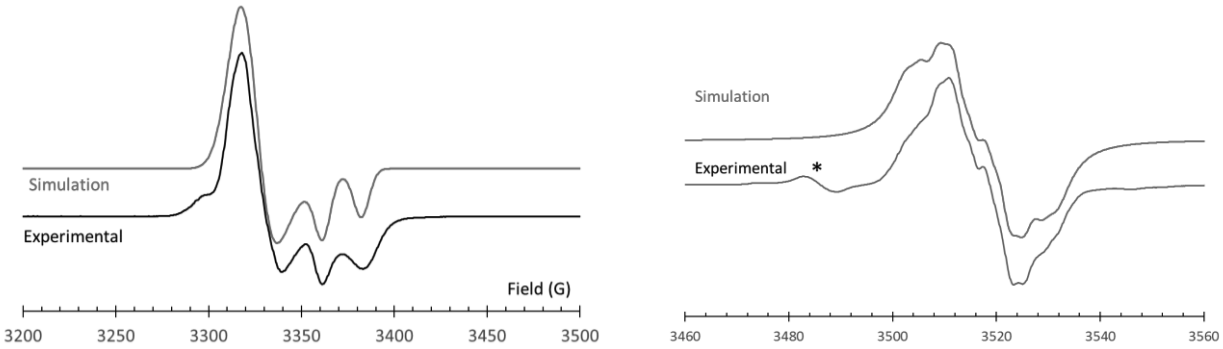

Figure 10. EPR spectrum of **7-Y** at 77 K (left); 298 K (right). Peak marked * is an unidentified impurity. Simulations based on data presented in Table 1.

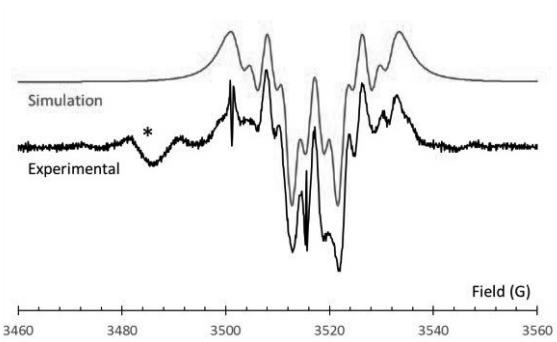

Figure 11. Second derivative EPR spectrum of **7-Y**. Peak marked * is an unidentified impurity. Simulation based on data presented in Table 1.

The solution spectrum is in marked contrast to other Y^{2+} complexes, such as $(Cp'_3Y)^{1-}$ (g = 1.991, A_Y = 36.6 G) which display simple doublets in solution due to coupling to ^{89}Y (100% abundant I = ½). The presence of additional hyperfine coupling and significantly reduced ^{89}Y hyperfine suggest more delocalization of the unpaired electron density onto the ligands in this product than in $(Cp'_3Y)^{1-}$.

Compound	$g_{\|}$	$g_{\perp}$	$A_{\|}$ (G)	$A_{\perp}$ (G)	g_{iso}	A (G)
7-Y	1.968	1.997	21.0	3.0*	1.983	8.7 (d), 6.4 (t), 2.9 (t)
9-Y	2.068	2.052	34.5	35.5	---	---

* unresolved. Value quoted is an upper limit based on linewidth

Table 1. EPR parameters for **7-Y**, and **9-Y**.

Attempts to crystallize the dark green product led only to the Ln^{3+} complex, [K(crown)]{[Cp'$_2$Y(μ–H)]$_3$(μ–H)}, **8-Y**, which was identified by X-ray crystallography, Figure 12. The X-ray data were not of high quality, but were sufficient to show that the anion in **8-Y** is analogous to those in the previously identified trimetallic tetrahydrides, [Li(THF)$_4$]{[($C_5H_4C_4H_9$)$_2$Er(μ–H)]$_3$(μ–H)}[19] and [Na(THF)]{[(C_5H_5)$_2$Lu(μ–H)]$_3$(μ–H)}.[20] Hence, although there is EPR evidence for a metal-based radical present in the yttrium system and UV-Vis data are similar to other Y^{2+} complexes, crystallographic evidence was not obtained to confirm a metal-metal bond.

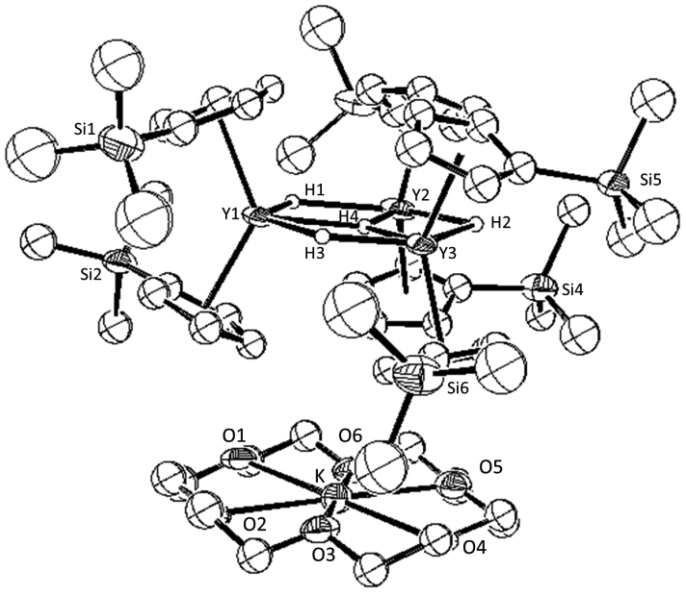

Figure 12. ORTEP depiction of [K(crown)]{[Cp'$_2$Y(μ–H)]$_3$(μ–H)}, **8-Y**, with thermal ellipsoids drawn at the 50% probability level. Hydrogen atoms, except for the bridging hydride ligands, have been omitted for clarity.

Reductions of **4-Dy** and **4-Tb** in Et_2O or THF with one equivalent of KC_8 in the presence of crypt or crown, also produced solutions that had the intense dark colors of previously identified Dy^{2+} and Tb^{2+} complexes, Figure 9.[3,4] Unfortunately, the solutions immediately began to lose their color before UV−vis spectra could be obtained. As in the yttrium case, crystallization attempts gave the Ln^{3+} polyhydrides [K(crypt)]{[Cp'$_2$Dy(μ–H)]$_3$(μ–H)}, **8-Dy**, and [K(crown)]{[Cp'$_2$Tb(μ–H)]$_3$(μ–H)}, **8-Tb**, which were identified by X-ray crystallography. As with **8-Y**, the crystal data were not of high quality. The **8-Ln** complexes could arise from ligand re-distribution upon decomposition of the Ln^{2+} solutions.[21,22] As has been seen in other studies of Ln^{2+} complexes, the specific ligand system is crucial to isolating single crystals of reduced species for crystallographic confirmation.

Reduction of a Bridging Chloride Complex. The reaction of [Cp'$_2$Y(μ–Cl)]$_2$, **1-Y**, with 1 equivalent of KC_8 in the presence of 2.2.2-cryptand at −35 °C in THF also yielded a dark purple/black solution, **9-Y**. The EPR spectrum of this product at 77 K and its simulation, Figure 13, show an axial signal with splitting characteristic of Y^{2+} (Table 1).[4,5,6] Although no room temperature spectrum was observed due to rapid sample decomposition at room temperature,[5] the isotropic spectral parameters (g = 2.057, A_Y = 35.2 G) estimated from the anisotropic parameters are similar to that of $(Cp'_3Y)^{1-}$ (g = 1.99 with A_Y = 36.6 G).[5,6] No crystallographically-characterizable products were isolated from this mixture in contrast to $(Cp'_3Y)^{1-}$ which readily crystallizes.[6] Hence, this chloride system appears to be too unstable to provide crystallographic evidence of metal-metal bonded species.

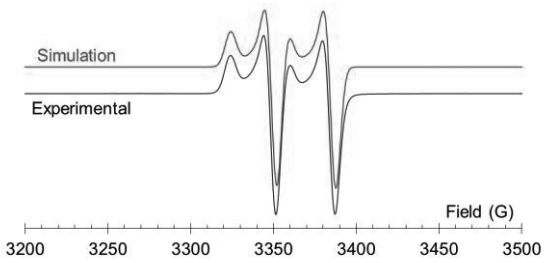

Figure 13. Frozen solution EPR spectra **9-Y**.

3. CONCLUSION

The reduction of $[Cp'_2Ln(\mu\text{–}H)(THF)]_2$, **4-Ln**, with potassium graphite gives EPR-active, intensely-colored solutions consistent with the formation of Ln^{2+} ions, but no crystallographic evidence of Ln^{2+} products was obtained from the dark solutions. Only the Ln^{3+} trimetallic tetrahydrides $[K(chelate)]\{[Cp'_2Ln(\mu\text{–}H)]_3(\mu\text{–}H)\}$ (chelate = 18-crown-6 or 2.2.2-cryptand; Ln = Y, Dy, Tb) were identifiable from the product mixture. Previous reductive studies of $(C_5H_5)_3Ln$, $(C_5H_4Me)_3Ln$, Cp''_3Ln, Cp''_2LnCp, and $(indenyl)_3Ln$ showed the importance of the ligand system for isolating crystals of complexes of Ln^{2+}. None of these other tris(cyclopentadienyl) ligand systems gave Ln^{2+} products that were as stable as the Cp'_3Ln reduction products. Evidently, bridging hydride or chloride ligands in conjunction with two Cp' ligands are not optimal for isolating crystallographically-characterizable new Ln^{2+} complexes, but this combination does lead to solutions which clearly reflect the spectroscopic properties of Ln^{2+} ions in systems that have the orbital characteristics for metal-metal bonding.

4. EXPERIMENTAL DETAILS

All manipulations and syntheses described below were conducted with the rigorous exclusion of air and water using standard Schlenk line and glovebox techniques under an argon or dinitrogen atmosphere. Solvents were sparged with UHP argon and dried by passage through columns

containing Q-5 and molecular sieves prior to use. Deuterated NMR solvents were dried over NaK alloy, degassed by three freeze-pump-thaw cycles, and vacuum transferred before use. ^{1}H NMR spectra and $^{13}C\{^{1}H\}$ NMR spectra were recorded on Bruker GN500 MHz spectrometer operating at 125 MHz for ^{13}C at 298 K unless otherwise stated and referenced internally to residual protio-solvent resonances. Elemental analyses were conducted on a Perkin-Elmer 2400 Series II CHNS elemental analyzer. UV-vis spectra were collected at 298 K using a Varian Cary 50 Scan UV-vis spectrophotometer. EPR spectra were collected using X-band frequency (9.3-9.8 GHz) on a Bruker EMX spectrometer equipped with an ER041XG microwave bridge, and the magnetic field was calibrated with DPPH (g = 2.0036). Potassium bis(trimethylsilyl)amide (Sigma-Aldrich) was purified by dissolving in toluene, centrifuging to remove insoluble material, and removing solvent from the supernatant. Allylmagnesium chloride (2.0 M solution in THF, Sigma-Aldrich), 1,4-dioxane (Sigma-Aldrich), and trimethylsilyl chloride (Alfa Aesar) were used as received. 2.2.2-cryptand (Sigma-Aldrich) and 18-crown-6 (Sigma-Aldrich) were placed under vacuum (10^{-3} Torr) before use. H_2 gas was used as received from Praxair. Anhydrous $LnCl_3$ (Ln = Y, Tb, Dy),[23] KC_8,[24] and $KC_5H_4(SiMe_3)$ (KCp')[25] were prepared according to the literature. $[Cp'_2Y(\mu\text{–}Cl)]_2$ was prepared by a modification of the literature procedure.[11]

$[Cp'_2Dy(\mu\text{–}Cl)]_2$, 1-Dy. In an argon-filled glovebox, a solution of KCp' (374 mg, 2.23 mmol) in diethyl ether (20 mL) was slowly added to a stirred solution of $DyCl_3$ (300 mg, 1.12 mmol) in diethyl ether (40 mL). The resulting cloudy colorless mixture was stirred in a warm water bath overnight. Diethyl ether was removed under vacuum and hexane (60 mL) was added to the colorless solids. The resultant colorless mixture was stirred in a warm water bath overnight. The solvent was removed under vacuum and the colorless solids were brought into a

glovebox free of coordinating solvents. The colorless solids were extracted with hexane (60 mL), and the slurry was centrifuged to remove colorless solids, presumably potassium chloride. The desired product was extracted from the colorless solids by centrifugation with additional hexane (40 mL). The supernatants were collected, combined, and the volatiles were removed under vacuum, yielding **1-Dy** as a colorless solid (0.360 g, 0.381 mmol, 68%). Colorless single crystals of **1-Dy** suitable for X-ray diffraction were grown from a concentrated solution of hexane at −35 °C overnight. IR: 3988w, 3971w, 3957w, 3941w, 3931w, 3793w, 3717w, 3653w, 3642w, 3551w, 3403w, 3174w, 3099w, 3083w, 3069w, 2953s, 2893m, 2796w, 2714w, 2669w, 2616w, 2552w, 2498w, 2474w, 2420w, 2384w, 2349w, 2266w, 2235w, 2148w, 2081w, 2001w, 1937w, 1873w, 1773w, 1736w, 1676w, 1665w, 1634w, 1578w, 1443s, 1405s, 1361s, 1322w, 1311m, 1245s, 1194w, 1174s, 1066m, 1042s, 906s, 850s, 837s, 786s, 779s, 757s, 747s, 690s, 631s. Anal. Calcd for $C_{32}H_{52}Si_4Dy_2$: C, 40.67; H, 5.55. Found: C, 41.04; H, 5.69.

[Cp'$_2$Tb(μ–Cl)]$_2$, 1-Tb. As described for **1-Dy**, $TbCl_3$ (300 mg, 1.20 mmol) and KCp' (400 mg, 2.40 mmol) were combined to produce **1-Tb** as light yellow solids (0.423 g, 0.457 mmol, 76%). Colorless single crystals of **1-Tb** suitable for X-ray diffraction were grown from a concentrated solution of hexane and toluene at −35 °C overnight. IR: 3972w, 3939w, 3794w, 3728w, 3655w, 3503w, 3177w, 3096w, 3085w, 3066w, 2950w, 2890m, 2793w 2712w, 2665w, 2616w, 2554w, 2474w, 2421w, 2348w, 2232w, 2151m, 2022w, 1937w, 1871w, 1769w, 1734w, 1673w, 1634w, 1579w, 1442s, 1403m, 1362s, 1322w, 1309w, 1245s, 1196w, 1173s, 1067w, 1067w, 1041s, 904s, 840s, 787s, 752s, 692s, 630s. Anal. Calcd for $C_{32}H_{52}Si_4Tb_2$: C, 40.98; H, 5.59. Found: C, 41.35; H, 5.54.

Cp'$_2$Y(η^3–C$_3$H$_5$)(THF), 2-Y. In a nitrogen-filled glovebox, **1-Y** (0.319 g, 0.400 mmol) was dissolved in toluene (20 mL) to yield a clear colorless solution. Allylmagnesium chloride

(2.0 M solution in THF, 0.400 mL, 0.800 mmol) was added dropwise, via a syringe, to the stirred solution. The resulting bright yellow solution was stirred overnight. Volatiles were removed under vacuum, and then hexane (15 mL) and 1,4-dioxane (0.2 mL) were added. The resulting yellow mixture was stirred for 3 h and centrifuged to remove colorless solids. The yellow supernatant was filtered and isolated. Additional product was extracted from the colorless solids by centrifugation with more hexane (20 mL). The yellow supernatants were combined and the solvent was removed under vacuum to yield **2-Y** as a crude yellow powder (0.337 g, 0.708 mmol). The crude yellow powder was crystallized from a concentrated hexane solution at −35 °C (0.225 g, 0.473 mmol, 60%) and identified as **2-Y**. Yellow crystals of **2-Y** suitable for X-ray diffraction were grown from a concentrated solution of hexane at −35 °C overnight. ^{1}H NMR (C_6D_6): δ 6.89 (p, J_{HH} = 12.5 Hz, 1H, $(CH_2)_2CH$), 6.48 (t, J_{HH} = 2.5 Hz, 4H, $C_5H_4SiMe_3$), 6.14 (t, J_{HH} = 2.5 Hz, 4H, $C_5H_4SiMe_3$), 3.51 (t, J_{HH} = 6.5 Hz, 4H, THF), 3.04 (d, J_{HH} = 10 Hz, 4H, $(CH_2)_2CH$), 1.30 (t, J_{HH} = 2.5 Hz, 4H, THF), 0.17 (s, 18H, $C_5H_4SiMe_3$). $^{13}C\{^{1}H\}$ NMR (C_6D_6): δ 150.95 $(CH_2)_2CH$, 127.9 ($C_5H_4SiMe_3$), 118.78 ($C_5H_4SiMe_3$), 112.37 ($C_5H_4SiMe_3$), 70.24 (THF), 63.74 [$(CH_2)_2CH$], 23.09 (THF), 0.04 ($C_5H_4SiMe_3$). IR: 3736w, 3683m, 3649w, 3070m, 2954s, 2899m, 2854w, 2802w, 2697w, 2554w, 2477w, 2411w, 2370w, 2250w, 2093w, 2005w, 1937w, 1873w, 1717w, 1685w, 1638w, 1545m, 1506w, 1456m, 1440s, 1403m, 1387w, 1362w, 1317m, 1251s, 1202m, 1176w, 1081s, 1045w, 1018w, 971w, 924s, 855s, 838s, 826s, 818s, 780s, 751s, 741s, 726m, 690s, 674s, 666s, 637s, 626s.

$Cp'_2Dy(\eta^3\text{–}C_3H_5)(THF)$, 2-Dy. As described for **2-Y**, **1-Dy** (0.235 g, 0.249 mmol) and allylmagnesium chloride (2.0 M solution in THF, 0.269 mL, 0.538 mmol) were combined to produce **2-Dy** as a yellow powder (0.272 g, 0.495 mmol). The crude yellow powder was crystallized from a concentrated hexane solution at −35 °C (0.211 g, 0.384 mmol, 77%) and

identified as **2-Dy**. Yellow crystals of **2-Dy** suitable for X-ray diffraction were grown from a concentrated solution of hexane and toluene at −35 °C overnight. IR: 3931w, 3920w, 3801w, 3683m, 3627m, 3608m, 3083m, 2952s, 2895s, 2851m, 2710w, 2670w, 2618w, 2551w, 2496w, 2472w, 2425w, 2353w, 2271w, 2237w, 2083w, 2001w, 1934w, 1872w, 1731w, 1640w, 1560w, 1548w, 1442s, 1403s, 1362s, 1311m, 1253s, 1243s, 1178s, 1133w, 1110w, 1098s, 1041s, 978w, 952w, 907s, 890w, 871s, 860s, 849s, 840s, 828s, 816s, 796s, 784s, 771s, 762s, 750s, 739s, 724s, 716m, 702m, 692s, 681m, 657m, 636s, 623s.

$Cp'_2Tb(\eta^3\text{–}C_3H_5)THF$, 2-Tb. As described for **1-Y**, **1-Tb** (0.384 g, 0.415 mmol) and allylmagnesium chloride (2.0 M solution in THF, 0.443 mL, 0.886 mmol) were combined to produce **2-Tb** as an orange/yellow oily solid (0.391 g, 0.716 mmol). The crude orange/yellow oil was crystallized from a concentrated hexane solution at −35 °C (0.261 g, 0.478 mmol, 58%) and identified as **2-Tb**. Yellow crystals of **2-Tb** suitable for X-ray diffraction were grown from a concentrated solution of hexane at −35 °C overnight. IR: 3925w, 3790w, 3679w, 3598w, 3079w, 2951s, 2893m, 2714w, 2667w, 2612w, 2551w, 2477w, 2421w, 2348w, 2083w, 1930w, 1873w, 1731w, 1641w, 1550w, 1442m, 1406w, 1359w, 1339w, 1309w, 1290w, 1247s, 1176s, 1129w, 1063w, 1039s, 1007w, 954w, 904m, 836s, 765s, 750s, 684m, 638m, 626m.

$[Cp'_2Y(\mu\text{–}H)]_3$, 3-Y. In a nitrogen-filled glove box, a Fischer-Porter high pressure apparatus was charged with solid yellow **2-Y** (0.086 g, 0.18 mmol), sealed, and attached to a high-pressure gas line. The pressure in the vessel was reduced to 0.5 atm and slowly charged with H_2 (60 psi) before being resealed and left overnight. The sample changed from yellow to colorless after 2 h. After 24 hours, residual hydrogen was removed under vacuum. The sample was transferred to an argon-filled glovebox and collected as a colorless solid (0.074 g, 0.0565 mmol, 95%) identified as **5-Y**. Colorless crystals of **5-Y** suitable for X-ray diffraction were

grown from a concentrated solution of hexane at −35 °C overnight. ^{1}H NMR (C_6D_6): δ 7.02 (t, J_{HH} = 2.5 Hz, 12H, $C_5H_4SiMe_3$), 6.45 (t, J_{HH} = 2.5 Hz, 12H, $C_5H_4SiMe_3$), 2.85 (t, J_{YH} = 32.5 Hz, 31H, Y–*H*), 0.23 (s, 54H, $C_5H_4Si\mathit{Me}_3$). $^{13}C\{^{1}H\}$ NMR (C_6D_6): δ 128.4 ($\mathit{C}_5H_4SiMe_3$), 118.71 ($\mathit{C}_5H_4SiMe_3$), 113.17 ($\mathit{C}_5H_4SiMe_3$), −0.66 ($C_5H_4Si\mathit{Me}_3$). IR: 3938w, 3790w, 3691w, 3598w, 3083m, 2952s, 2893s, 2849m, 2714w, 2667w, 2614w, 2554w, 2481w, 2383w, 2346w, 2239w, 2087w, 2003w, 1937w, 1874w, 1721w, 1631w, 1442s, 1404s, 1362s, 1309w, 1248s, 1178s, 1102w, 1040s, 979w, 908s, 837s, 769s, 750s, 688s, 640s, 626s.

[Cp'$_2$Dy(μ–H)(THF)]$_2$, 4-Dy. As described for **3-Y**, **2-Dy** (0.106 g, 0.193 mmol) was reacted in a Fischer-Porter apparatus charged with H_2 gas (60 psi) for 24 hours to produce a white solid (0.098 g, 0.096 mmol, 99 %) identified as **4-Dy**. Colorless crystals of **4-Dy** suitable for X-ray diffraction were grown from a concentrated solution of hexane and toluene at −35 °C overnight. IR: 3927w, 3685w, 3647w, 3600w, 3409w, 3086w, 2954s, 2895m, 2714w, 2672w, 2618w, 2481w, 2348w, 2085w, 2001w, 1932w, 1871w, 1718w, 1631w, 1444s, 1403s, 1361s, 1311m, 1247s, 1178s, 1043s, 9745w, 906s, 840s, 773s, 754s, 686m, 640m, 628m.

[Cp'$_2$Tb(μ–H)(THF)]$_2$, 4-Tb. As described for **3-Y**, **2-Tb** (0.240 g, 0.439 mmol) was reacted in a Fischer-Porter apparatus charged with H_2 gas (60 psi) for 24 hours to produce a white solid (0.214 g, 0.211 mmol, 96.2 %) identified as **4-Tb**. Colorless crystals of **4-Tb** suitable for X-ray diffraction were grown from a concentrated solution of hexane at −35 °C overnight. IR: 3675w, 3657w, 3606m, 3081w, 3063w, 2952s, 2893m, 2710w, 2391w, 2267w, 2087w, 1932w, 1869w, 1634w, 1440m, 1403w, 1362m, 1247s, 1174s, 1129w, 1041s, 904s, 829s, 775s, 750s, 686m, 636s.

[Cp'$_2$Y(THF)]$_2$(μ–O), 5-Y. 2-Y (0.168 g, 0.353 mmol) was dissolved in hexane (8 mL) in a 100 mL Teflon sealable Schlenk type flask. The bright yellow solution was degasses

through three freeze, pump, thaw cycles. The flask was stirred in an ice bath and charged with 1 atm of H_2 gas, was allowed to stir for 25 minutes, after which the solution was clear and colorless. The flask was degassed and charged with H_2 gas a total of three times. The solvent was removed under vacuum. The product was isolated as a colorless solid (0.140 g, 0.158 mmol). The product was crystalized in minimal hexane and toluene. Colorless single crystals of **4** suitable for X-ray diffraction were grown from a concentrated solution of hexane at −35 °C overnight. ^{1}H NMR (C_6D_6): δ 6.72 (t, J_{HH} = 2.5 Hz, 8H, $C_5H_4SiMe_3$), 6.31 (t, J_{HH} = 2.5 Hz, 8H, $C_5H_4SiMe_3$), 0.28 (s, 36H, $C_5H_4SiMe_3$).

[Cp'$_2$Dy(μ−H)]$_3$, 3-Dy. In an argon-filled glovebox white, **4-Dy** (185 mg, 0.181 mmol) was placed in a sublimation tube, sealed, and placed on a high vacuum line. The sample was placed under vacuum (10^{-5} Torr), while heating at 70 °C for 4 days. The product was isolated as an off-white, light yellow solid (0.160 g, 0.183 mmol), identified as **3-Dy**. Colorless single crystals suitable for X-ray diffraction were grown from a concentrated solution of hexane and toluene at −35 °C. IR: 3938w, 3683m, 3606m, 3542w, 3407w, 3083m, 2952s, 2895s, 2714w, 2667w, 2616w, 2556w, 2494w, 2474w, 2421w, 2385w, 2351w, 2235w, 2087w, 1997w, 1932w, 1874w, 1714w, 1603m, 1444s, 1401s, 1361s, 1311s, 1252s, 1176s, 1041s, 904s, 852s, 821s, 789s, 759s, 687s, 638s, 628s. Anal. Calcd for $C_{48}H_{81}Si_6Dy_3$: C, 43.87; H, 6.21. Found: C, 43.65; H, 6.16.

[Cp'$_2$Tb(μ−H)]$_3$, 3-Tb. In an argon-filled glovebox, **4-Tb** (317 mg, 0.313 mmol) was placed in a sublimation tube, sealed, and placed on a high vacuum line. The sample was placed under vacuum (10^{-5} Torr), while heating at 55 °C for 5 days. The product was isolated as an off-white solid (266 g, 0.306 mmol), identified as **3-Tb**. Colorless single crystals suitable for X-ray diffraction were grown from a concentrated solution of hexane and toluene at −35 °C. IR:

3940w, 3653m, 3086s, 2944s, 2897s, 2856m, 2710w, 2667w, 2618w, 2556w, 2479w, 2348w, 2230w, 2086w, 1939w, 1874w, 1725w, 1632w, 1444s, 1406s, 1362s, 1311s, 1245s, 1178s, 1048s, 902s, 870s, 842s, 814s, 789s, 765s, 748s, 720s, 698s, 638s, 628s. Anal. Calcd for $C_{48}H_{81}Si_6Tb_3$: C, 44.23; H, 6.26. Found: C, 44.04; H, 6.22.

[K(18-crown-6)]{[Cp'$_2$Y(μ^2–H)]$_3$(μ^3–H)}, 8-Y, from 3-Y. In an argon-filled glovebox, **3-Y** (90.5 mg, 0.103 mmol), and 2.2.2 cryptand (39 mg, 0.10 mmol) were combined, and dissolved in THF (1.5 mL). This solution was slowly added to a stirring slurry of KC_8 (14 mg, 0.10 mmol) in THF (0.5 mL). After the solution was added, it quickly became a dark green. The solution was allowed to stir for 4 minutes and was filtered to remove a black precipitate, presumably graphite. The dark green filtrate was layered with pentane and placed in a freezer at −35 °C overnight to produce a dark green oily solid. The product was isolated as a tacky green solid (110 mg). Dark green single crystals identified as **5-Y**, could be grown from a concentrated solution of Et_2O layered with pentane at −35 °C, or from a vapor diffusion of pentane into a concentrated solution of Et_2O at −15 °C. IR: 3703w, 3081w, 2953m, 2888m, 2811m, 1558w, 1478w, 1457w, 1444w, 1407w, 1356m, 1298w, 1258m, 1240m, 1182m, 1135m, 1105s, 1082m, 1061w, 1038m, 1019w, 1011w, 993w, 950m, 932m, 906m, 884w, 868w, 830s, 786w, 755s, 748s, 740m, 731m, 715w, 706w, 695w, 686w, 675w, 665w, 650w, 639w, 632w, 624w, 616w. UV-vis (THF) λ_{max} = 794 nm; ε = 1000 $M^{-1}cm^{-1}$.

[K(2.2.2-cryptand)]{[Cp'$_2$Dy(μ–H)]$_3$(μ^3–H)}, 8-Dy, from 4-Dy. In an argon-filled glovebox, **4-Dy** (77 mg, 0.075 mmol), and 2.2.2 cryptand (28 mg, 0.075 mmol) were combined, and dissolved in THF (3 mL). This solution was slowly added to a stirring slurry of KC_8 (10 mg, 0.075 mmol) in THF (0.5 mL). After the solution was added, it quickly became a dark blue. The solution was allowed to stir for 3 minutes and filtered to remove a black precipitate, presumably

graphite. The dark blue filtrate was layered with pentane and placed in a freezer at −35 °C overnight to produce a dark blue oily solid. Dark black single crystals identified as **5-Dy**, could be grown from a concentrated solution of ether layered with pentane, or from a vapor diffusion of pentane into a concentrated solution of ether at −15 °C. IR: 3706w, 3096w, 3081w, 3066w, 2952, 2886s, 2819.42m, 2762w, 2728w, 2620w, 2498w, 2359w, 2091w, 1930w, 1869w, 1604w, 1477m, 1459m, 1444m, 1403w, 1361s, 1297m, 1242s, 1180s, 1134s, 1106s, 1077s, 1059m, 1039s, 987w, 952s, 932m, 907s, 830s, 770s, 751s, 686m, 643m, 626s. UV-vis (THF) λ_{max} = 715 nm; ε = 640 $M^{-1}cm^{-1}$.

[K(18-crown-6)]{[Cp'$_2$Tb(μ−H)]$_3$(μ^3−H)}, 8-Tb, from 4-Tb. In an argon-filled glovebox, **4-Tb** (101 mg, 0.0977 mmol) and 2.2.2 cryptand (26 mg, 0.10 mmol) were combined, and dissolved in ether (2 mL). The solution was slowly added to a stirring slurry of KC_8 (14 mg, 0.10 mmol) in ether (0.5 mL). After the solution was added, it quickly became dark blue. The solution was allowed to stir for 4 minutes and filtered to remove a black precipitate, presumably graphite. The dark blue filtrate was layered with pentane and placed in a freezer at −35 °C overnight to produce a dark green oily solid. Dark blue single crystals identified as **5-Tb**, were grown from a concentrated solution of ether layered with pentane at −15 °C. IR: 3705m, 3083m, 2954s, 2897s, 2826m, 2793w, 1662w, 1495w, 1471m, 1443m, 1405w, 1353m, 1311w, 1284w, 1245s, 1182m, 1112s, 1069w, 1037s, 986w, 963m, 945w, 932w, 907s, 889w, 867m, 838s, 826s, 774s, 764s, 750s, 738m, 725m, 694m, 640m, 626m. UV-vis (THF) λ_{max} = 837 nm; ε = 840 $M^{-1}cm^{-1}$.

X-ray Crystallographic Data. Crystallographic information for complexes **1-Dy**, **1-Tb**, **2-Y**, **2-Dy**, **2-Tb**, **3-Y**, **3-Dy**, **3-Tb**, **4-Dy**, **4-Tb**, **5-Y**, **6-Tb**, **8-Y**, **8-Dy**, **and 8-Tb** is summarized in the Supporting Content.

Computational Details. DFT calculations were performed using the TPSS[26] meta-generalized gradient approximation (meta-GGA) functional with Grimme's D3 dispersion correction.[27,28] Initial geometry optimizations were carried out using basis sets of valence double-zeta quality with polarization functions on nonhydrogen atoms, def2-SV(P).[29] Numerical vibrational normal mode analyses were performed to confirm that the optimized structures are minima on the ground-state potential energy surface. Starting from each optimized structure, a second geometry optimization was performed using basis sets of valence triple-zeta quality plus polarization, def2-TZVP.[30] Both geometry optimizations were performed in C_1 symmetry till the Cartesian coordinate gradient was converged to $\leq 10^{-4}$ a.u. The 28 core electrons of yttrium were modeled by Stuttgart-Cologne scalar-relativistic effective core potential (ECP).[31] Fine density grids of at least m4 quality[32] were employed for numerical integration. Solvent effects were included by the continuum solvation model (COSMO)[33] using the dielectric constant of THF ($\varepsilon = 7.52$).[34] Boys orbital localization[10] was performed for the highest 11 occupied orbitals (1 Y–Y bond, 8 $(Cp')^{1-}$ π_2, and 2 H 1s) of $\{[Cp'_2Y(\mu\text{–}H)]_2\}^{2-}$. All calculations were performed using TURBOMOLE 7.0.[35]

EPR Spectroscopy. EPR spectra were collected using X-band frequency (9.3-9.8 GHz) on a Bruker EMX spectrometer equipped with an ER041XG microwave bridge and the magnetic field was calibrated with DPPH ($g = 2.0036$). Solution EPR spectra were simulated using WINSIM[17] whereas frozen spectra were simulated using PIP4WIN.[18]

AUTHOR INFORMATION

Corresponding Author

*E-mail: wevans@uci.edu

ACKNOWLEDGMENTS

We thank the U.S. National Science Foundation for support of the experimental studies (CHE-1565776 to W.J.E) and the theoretical studies (CHE-1464828 to F.F.). J.M.R. and M.A.N. would like to thank the Canada Research Chairs program and NSERC, respectively, for financial support and particularly the NSERC Michael Smith Foreign Study Award for M.A.N. We also thank Professor A. S. Borovik for assistance with EPR and UV-vis spectroscopy.

Appendix A. Supplementary data

Computational details, selected bond distances, and crystallographic data (CIF) for **11-Dy**, **1-Tb**, **2-Y**, **2-Dy**, **2-Tb**, **3-Y**, **3-Dy**, **3-Tb**, **4-Dy**, **4-Tb**, **5-Y**, **6-Tb**, **7-Y**, **7-Dy**, **and 7-Tb** are available free of charge via the Internet. Crystallographic data for complexes **1-Dy** (CCDC no. 1529527), **1-Tb** (1529518), **2-Y** (1529515), **2-Dy** (1529519), **2-Tb** (1529520), **3-Y** (1529517), **3-Dy** (1529529), **3-Tb** (1529528), **4-Dy** (1529521), **4-Tb** (1529523), **5-Y** (1529516), **6-Tb** (1529522), **8-Y** (1529524), **8-Dy** (1529525), **8-Tb** (1529526) can be obtained free of charge from The Cambridge Crystallographic Data Centre via www.ccdc.cam.ac.uk/data_request/cif.

Table of Contents Graphic:

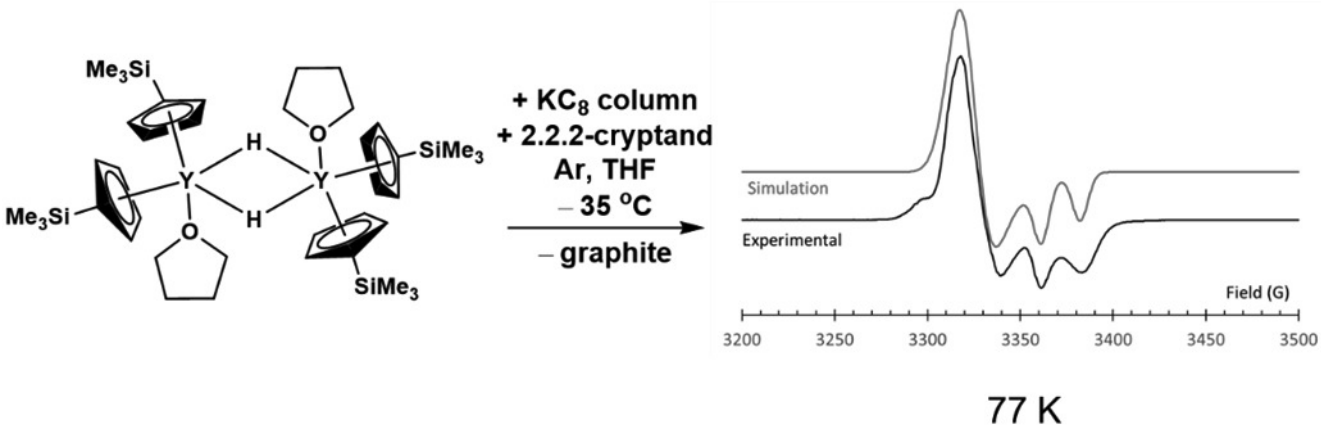

REFERENCES

(1) Hitchcock, P. B; Lappert, M. F; Maron, L.; Protchenko, A. V. *Angew. Chem., Int. Ed.* **2008**, *47*, 1488-1491.
(2) Macdonald, M. R.; Bates, J. E.; Ziller, J. W.; Furche, F.; Evans, W. J. *J. Am. Chem. Soc.* **2013**, *135*, 9857-9868.
(3) MacDonald, M. R.; Bates, J. E.; Fieser, M. E.; Ziller, J. W.; Furche, F., Evans, W. J. *J. Am. Chem. Soc.* **2012**, *134*, 8420-8423.
(4) Fieser, M. E.; MacDonald, M. R.; Krull, B. T.; Bates, J. E.; Ziller, J. W.; Furche, F.; Evans, W. J. *J. Am. Chem. Soc.* **2015**, *137*, 369-382.
(5) Corbey, J. F.; Woen, D. H.; Palumbo, C. T.; Fieser, M. E.; Ziller, J. W.; Furche, F.; Evans, W. J. *Organometallics* **2015**, *34*, 3909-3921.
(6) MacDonald, M. R.; Ziller, J. W.; Evans, W. J. *J. Am. Chem. Soc.* **2011**, *133*, 15914-15917.
(7) Ortiz, J. V.; Hoffmann, R. *Inorg. Chem.* **1985**, *24*, 2095-2104.
(8) Venanzi, L. M. *Coord. Chem. Rev.* **1982**, *43*, 251-274.
(9) Evans, W. J.; Meadows, J. H.; Wayda, A. L.; Hunter, W. E.; Atwood, J. L. *J. Am. Chem. Soc.* **1982**, *104*, 2008-2014.
(10) Foster, J. M.; Boys, S. F. *Rev. Mod. Phy.* **1960**, *32*, 300-302.
(11) Evans, W. J.; Sollberger, M. S.; Shreeve, J. L.; Olofson, J. M.; Hain, J. H. *Jr.*; Ziller, J. W. *Inorg. Chem.* **1992**, *31*, 2492-2501.
(12) Peterson, J. K.; MacDonald, M. R.; Ziller, J. W.; Evans, W. J. *Organometallics* **2013**, *32*, 2625-2631.
(13) Spirlet, M.-R.; Goffart, J. *J. Organomet. Chem.* **1995**, *493*, 149-151.
(14) Satoh, Y.; Ikitake, N.; Nakayama, Y.; Okuno, S.; Yasuda, H. *J. Organomet. Chem.* **2003**, *667*, 42-52.
(15) Evans, W. J.; Drummond, D. K.; Hanusa, T. P. Doedens, R. J. *Organometallics*, **1987**, *6*, 2279-2285.
(16) Clark, E. P. *Ind. Eng. Chem. Anal. Ed.* **1941**, *13*, 820-821.
(17) Duling, D. R. *J. Magn. Reson., Ser B* **1994**, *104*, 105-110.
(18) (a) M. Nilges, Illinois, EPR Research Centre; (b) PIP4WIN v. 1.2, J.M. Rawson, University of Windsor (2011).
(19) Yao, T.; Song, S.; Shen, Q.; Hu, J.; Lin, Y. *Chin. Sci. Bull.* **2004**, *49*, 1578.
(20) Protchenko, A. V.; Fedorova, E. A.; Bochkarev, M. N.; Schumann, H.; Loebel, J.; Kociok-Kohn, G. *Russ. Chem. Bull.* **1994**, 2027.
(21) La Pierre, H.S.; Kameo, H.; Halter, D.P.; Heinemann, F.W.; Meyer, K. *Angew. Chem., Int. Ed.* **2014**, *53*, 7154-7157.
(22) Gun'ko, Y.K.; Hitchcock, P.B.; Lappert, M.F. *Organometallics* **2000**, *19*, 2832-2834.
(23) Taylor, M. D. *Chem. Rev.* **1962**, *62*, 503-511.
(24) Bergbreiter, D. E.; Killough, J. M. *J. Am. Chem. Soc.* **1978**, *100*, 2126-2134.
(25) Peterson, J. K.; MacDonald, M. R.; Ziller, J. W.; Evans, W. J. *Organometallics* **2013**, *32*, 2625-2631.
(26) Tao, J.; Perdew, J.; Staroverov, V.; Scuseria, G. *Phys. Rev. Lett.* **2003**, *91,* 146401-146404.
(27) Grimme, S. *J. Comput. Chem.* **2006**, *27*, 1787-1799.
(28) Grimme, S.; Antony, J.; Ehrlich, S.; Krieg, H. *J. Chem. Phys.* **2010**, *132*, 154104-154119.
(29) Schäfer, A.; Schuurmann, G. *J. Chem. Phys.* **1993**, *97*, 2571-2577.
(30) Weigend, F.; Ahlrichs, R. *Phys. Chem.* **2005**, *7*, 3297-3305.
(31) Andrae, D.; Haubermann, U.; Dolg, M.; Stoll, H.; Preuss, H. *Theoret. Chim. Acta*, **1990**, *77*, 123-141.
(32) Treutler, O.; Ahlrichs. R. *J. Chem. Phys.* **1995**, *102*, 346-354.
(33) Klamt, A.; Schüürmann G. *J. Chem. Soc., Perkin Trans.* **1993**, *2*, 799-805.
(34) CRC Handbook of Chemistry and Physics; 88th ed.; Lide, D. R., Ed.; CRC Press: Boca Raton, 2008; Chapter 8, p 136